JOURNAL OF CHEMICAL EDUCATION

pubs.acs.org/jchemeduc

Technology Report

Low-Cost Multispectral Imager

Annemarie McCarthy,* Killian Barton, and Liam Lewis

Cite This: J. Chem. Educ. 2020, 97, 3892–3898

Read Online

ACCESS | Metrics & More | Article Recommendations | Supporting Information

ABSTRACT: A low-cost multispectral imager was built using a multiwavelength LED PCB (light-emitting diode printed circuit board), 3D printed housing, and a monochrome camera, and it was controlled via National Instruments LabVIEW software coupled with some simple electronics. Multivariate data analysis was performed using freely available software packages. The device is sufficiently simple in its construction and operation to be of use in many undergraduate courses concerned with topics such as spectroscopy, chemometrics, and colorimetry.

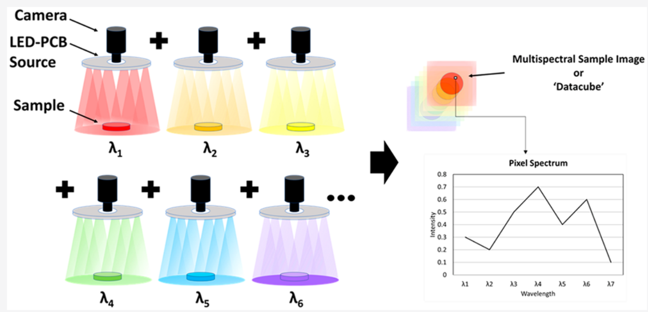

KEYWORDS: *First-Year Undergraduate/General, Second-Year Undergraduate, Upper-Division Undergraduate, Graduate Education/Research, Interdisciplinary/Multidisciplinary, Laboratory Instruction, Hands-On Learning/Manipulatives, Instrumental Methods, Spectroscopy, Chemometrics*

INTRODUCTION

Multispectral imaging is the process whereby light intensity is recorded as a function of wavelength at each spatial position or pixel of an image. The spectral data at each point allows each pixel to be identified and sorted according to its spectral fingerprint. This is useful for a wide range of applications, examples of which include medical imaging, online process analysis, machine vision, and surveying.[1−4] The optical spectrum can be collected across a wide range of wavelengths including UV, visible, near-infrared, and mid-infrared. The range in the electromagnetic spectrum from which the spectral data is recorded will determine the type of physical and chemical information being revealed about the sample. The terminology in the field is subject to some inconsistency, with the terms spectral, multispectral, and hyperspectral being used almost interchangeably.[5] In general, however, multispectral imaging refers to the capture of a spectrum with few (ca. 10) bands at each pixel while hyperspectral imaging refers to the capture of a spectrum with many (>100) bands.

Capturing spectral information while imaging a sample is a somewhat complex process. This can be illustrated by examining two different multispectral imaging approaches. The first approach is to record the sample image using a filter-wheel camera.[6,7] The multispectral data cube is recorded by combining images captured using a sequence of bandpass filters. This is referred to as a "staring image" technique and requires that the sample or scene is static or unchanging during acquisition. A similar staring image technique is available on the basis of acousto-optic tunable filters.[8] The second technique is to record the sample image using push-broom imaging.[9] This technique is defined by the sensor architecture, where a linear array of filters separates the light at each pixel by wavelength to a perpendicular array of sensor pixels. This requires that the sample moves through the plane of view of the array, for example, on a conveyer belt. Alternatively, the camera is scanned across the scene as in the case of satellite multispectral and hyperspectral imaging of the earth's surface. The hardware required for traditional multispectral imaging methods such as these is costly. Push-broom imaging systems tend to cost upward of €80,000. A 12-position motorized filter wheel combined with filters alone may cost upward of €3,000.[6,10] There are many other system designs for multispectral and hyperspectral imaging which are not covered here but may be of interest. These include nonscanning or "snapshot" systems which can capture the whole data cube within a single integration period, using, for example, faceted mirrors or lenslet arrays to disperse both the spatial and spectral elements of the image over the area of the detector.[5,11]

The multispectral imaging technique presented in this article is an adaptation of the filter-wheel camera. Instead of filtering the light reflected from a sample, the sample is illuminated with a series of LEDs, each with a discrete wavelength of emission. An image is captured at each wavelength by a monochrome camera, and the series of images is combined to form the multispectral data cube. A number of devices of this general type have been

Received: April 27, 2020
Revised: August 5, 2020
Published: August 31, 2020

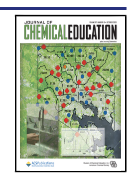

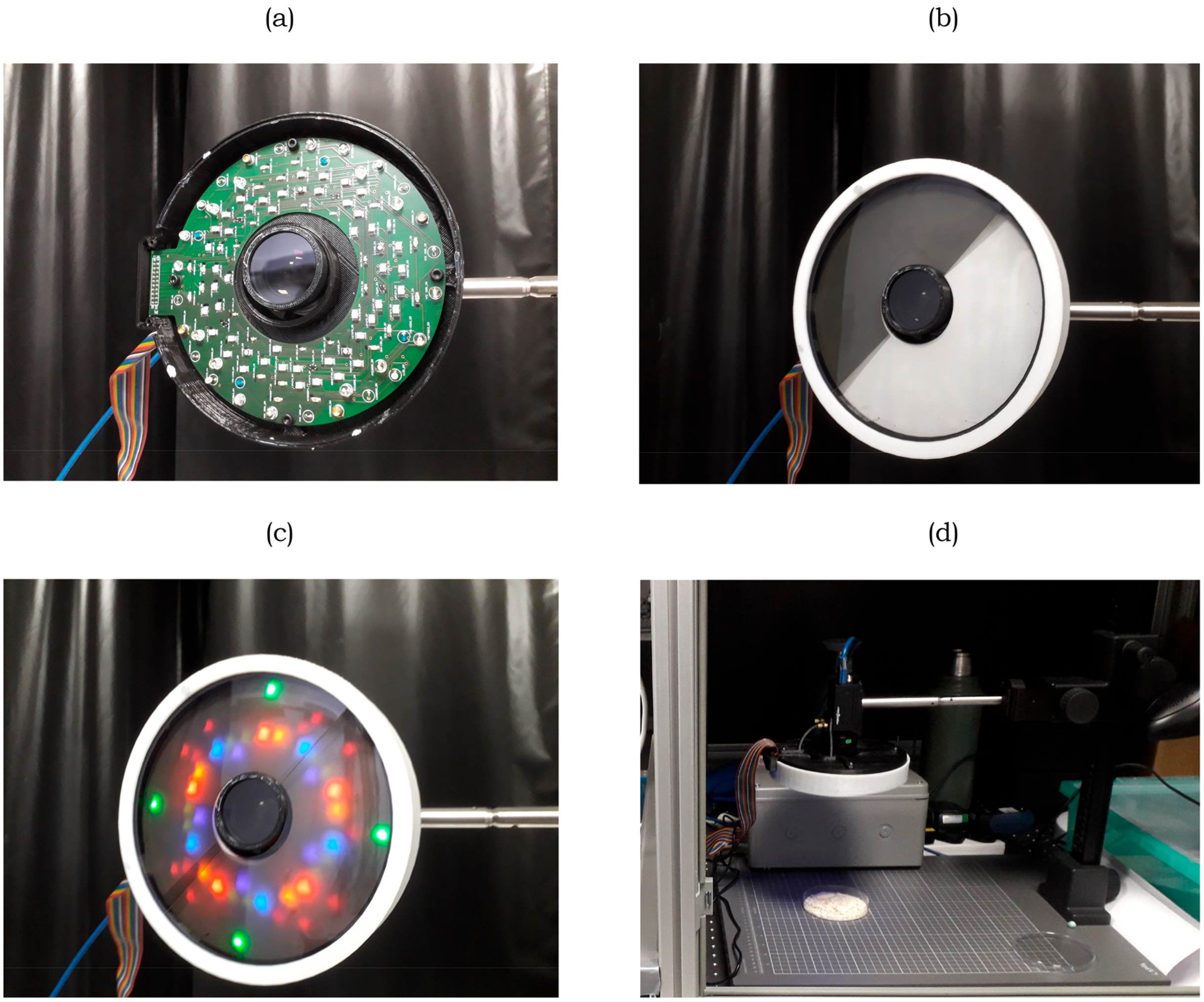

Figure 1. (a) MSI with front cover and optical components removed. The LED PCB is visible. The camera lens is located at the center of the instrument. (b) The MSI with diffuser and polarizer added, with the latter shown partially inserted. (c) The MSI fully assembled with LED array fully illuminated. During actual use, the LEDs are illuminated sequentially. (d) The MSI assembly viewed edge-on. The camera is attached to an optical post, and the lighthead is mounted via a 3D printed strut on the camera body.

previously described[12−15] with specific applications ranging from biomedical (e.g., the measurement of diffuse reflectance spectra from human skin[12]) to cultural (the digitization of historical documents[13]). Data analysis methods described in the literature include simple cataloging and manual inspection of images[13,15] and the use of custom developed algorithms[14] and software.[12,14] The device described here is a general-purpose multispectral imaging tool, which is inexpensive, robust, and intuitive in its use, requiring no moving parts, complex setup, or calibration. Data acquisition and analysis is performed using widely available software packages, and its construction is described in detail (see Supporting Information) to facilitate its easy replication.

It is suitable for application to a wide range of imaging and sample analysis tasks. Many undergraduate and postgraduate courses include the topics of spectroscopy,[16−18] chemometrics,[19−22] and colorimetry.[23,24] The multispectral imager (MSI) described here could be a useful teaching aid for many of these courses. At an introductory level, it provides an intuitive and hands-on way for students to understand the basics of spectroscopy, while at a more advanced level it provides opportunities for students to develop skills in the essential chemometric multivariate analysis techniques of principal component analysis and k-means clustering. The assembly of the imager and the design and integration of the electronics, hardware, and software could also be a useful exercise in the development of student knowledge of engineering and automation, which have been identified as useful skills for students of chemistry.[25,26] In this context, the MSI described here was used at Cork Institute of Technology as the basis of a final year undergraduate project investigating its application in the analysis of skin samples, and the design of an alternative electronic control method for the imager formed the basis of a project for a module teaching the fundamentals of the Arduino platform.

ASSEMBLY OF MSI

The MSI consists of an illuminator (comprising LEDs, diffuser, polarizer (optional), and lens (optional)), camera, and associated control electronics and software. The illuminator contains chains of LEDs, each operating at a different wavelength. The system operates by powering the LED channels one by one and taking an image of the target at each wavelength.

Optics

The MSI uses a coaxial diffuse light source to provide uniform nondirectional lighting on the target area. Each component is described below. The illuminator components are housed inside a custom designed unit which was 3D printed in-house. The total cost of the unit (choosing cost-effective camera and lens as discussed below) is approximately €885, of which the lens and camera account for €600.

LEDs. The MSI has 18 wavelength channels, and the LEDs were mounted on a doughnut shaped PCB (printed circuit board, see Figure 1), with care taken to ensure an even spread of each wavelength's LED around the circumference. In addition, where possible, LEDs from a particular wavelength were all mounted at the same distance from the virtual center of the PCB, to ensure beam symmetry when used in conjunction with the (optional) lens. The number of each type of LED used was chosen on the basis of irradiance/illuminance values, camera sensor sensitivity, and transmission of optical components, to achieve a similar detector response for each wavelength. A minimum number of four LEDs per wavelength was used, to ensure beam symmetry. They were operated in the pulsed mode with each chain typically turned on for 300−500 ms per image cycle. This allowed for higher currents to be used, thereby achieving higher irradiance levels on the target plane. Further details of the LEDs can be found in the Supporting Information.

Diffuser. A diffuser (see Figure 1) (Brightview CHE-30) was used to flatten and smooth the irradiance pattern on the target surface.

Polarizer (Optional). A polarizer (see Figure 1) can be employed to reduce the intensity of surface reflections in the images. A linear dichroic polymer film polarizer is most convenient, as it can be cut to the size of the PCB and camera lens. Edmund Optics (45-668) is a suitable choice, providing appropriate polarization over the wavelength range 400−700 nm. [Unfortunately, achieving wider coverage requires a far more costly solution e.g., the Boldervision BVO 1000 linear polarizer (approximately $1500).] The PCB and camera lens polarizers must be crossed to effectively eliminate surface reflections.

Lens (Optional). A Fresnel lens (e.g., Edmund Optics 46-614) can be fitted to the unit to reduce the diameter of the beam and increase intensity, for applications requiring a small field of view.

Camera. A Point Gray camera (GS3-U3-41C6NIR-C) with a 1 in. NIR enhanced sensor (QE ∼ 15% at 900 nm) was used to maximize the sensitivity of the instrument in the NIR (providing additional QE in the 700−1050 nm range). However, a significant cost saving can be achieved through the use of a standard CCD or CMOS digital camera with a 1/2 in. (or 1/3 in.) monochrome sensor (e.g., PG CM3-U3-13Y3M with ON Semi P1300 sensor (QE ∼ 7% at 900 nm)). Choice of camera lens is dictated primarily by desired field of view, and sensor size. In this implementation, a Navitar MVL16M1 was used (e.g., Thorlabs MVL16M23 is a suitable cost-effective choice for the Point Gray Chameleon camera suggested above.)

Electronics and Control Software

The LEDs of each channel are mounted in series, powered by an external 24VDC power supply, and switched by means of a series of transistors whose base bins are connected to an NI digital I/O card (see Figure 2). A potentiometer was also placed in each chain. The control software was compiled in National Instruments LabVIEW. Full details of all components used, as well as PCB design files, and the LabVIEW control software are provided in the Supporting Information.

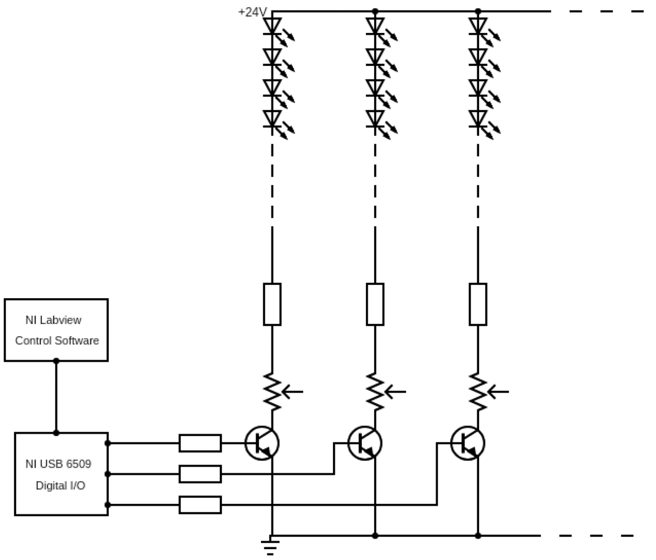

Figure 2. Schematic of electronic control scheme for the MSI. Three chains of LEDs are shown. Eighteen LED channels, arranged in 20 chains were used in the actual device. The dashed lines on the upper and lower right-hand side indicate this. Full details of the components used, and schematics are contained in the Supporting Information.

An alternative control scheme was also tested, where the transistors were connected to the output of a shift register, controlled by an Arduino microcontroller. This control scheme also worked well and could provide an additional opportunity for students to develop instrumentation and electronic knowledge and skills. Further details are provided in the Supporting Information.

Data Analysis

Preparing the Data. Preparing the data cube from the images recorded using the LED MSI can be achieved using Hypercube. Hypercube is an open source spectral image analysis software package, published by the US Geospatial Research Laboratory and the US Engineer Research and Development Center.[27] To construct the data cube using Hypercube, the following steps are necessary:

- Convert the .bmp images captured using the LED MSI to .jpeg. This can be carried out rapidly by using an open source tool such as "Bulk Image Converter".
- Open each image in Hypercube and use the "convert color to h, s, i" function to extract the intensity image for each wavelength. Save the intensity image to a new folder.
- Open the intensity images in Hypercube and use the "plane to cube" function to begin compiling the hypercube. Begin with the 405 nm image. For each subsequent image, use the "add to cube" function to include it in the data cube.
- After adding the images to the cube, save the cube as a .bil file.

Analyzing the Data. The data cube prepared using Hypercube can be explored in Spectronon, an open source imaging tool.[28] k-Means cluster analysis and principal component analysis (PCA) are both offered in this software. SIMCA classification can also be performed on the basis of the results of these analyses. These techniques are well-known

Figure 3. From left: (a) Pantone D65 color card under sunlit conditions (b), MSI image at 633 nm (red), (c) MSI image at 740 nm (infrared), and (d) cluster analysis.

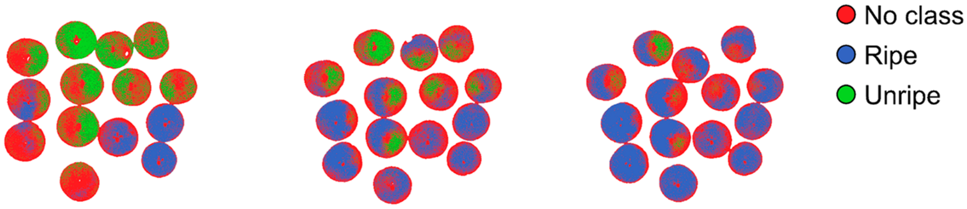

Figure 4. Application of the results from PCA of the vine tomato images to classification modeling. The SIMCA model identifies each pixel as either a ripe, unripe, or unclassified site on tomatoes in the image. The images, from left to right, represent day 1, day 4, and day 7 of the ripening study.

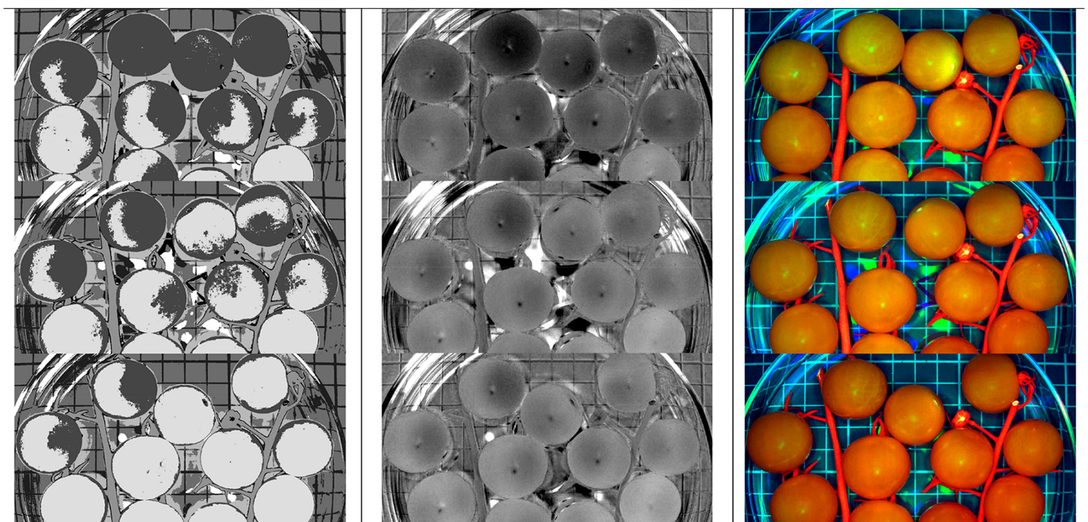

K Means Clustering	PCA:	LED Imaging:
	Component 3	RGB;
		870 nm (R), 586 nm(G),
		470 nm (B)

Figure 5. Vine tomato ripening, with results from clustering and PCA of multispectral images taken of tomato samples. The samples, from top to bottom in each image, are from day 1, day 4, and day 7 of the ripening study.

unsupervised machine learning techniques used to classify and reduce the dimensionality of data.[29−31]

Performance

Metamerism. Metamerism is a phenomenon whereby colors with different spectral power distributions are indistinguishable to the human eye. Color perception in the human eye is governed by the spectral sensitivities of the three different

https://dx.doi.org/10.1021/acs.jchemed.0c00407
J. Chem. Educ. 2020, 97, 3892−3898

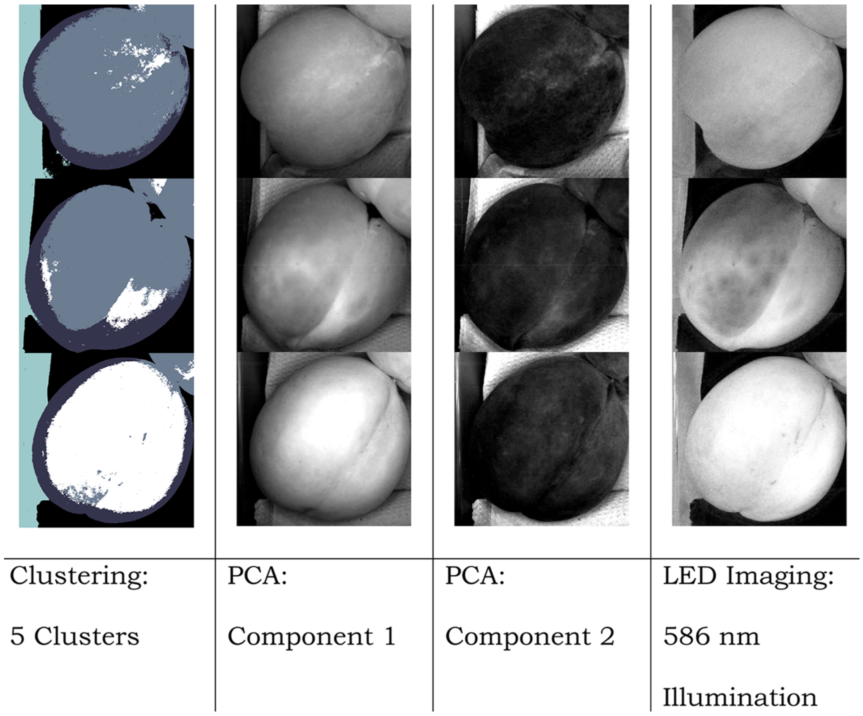

Figure 6. Peach chill injury, with results from clustering and PCA of multispectral images taken of peach samples. The samples, from top to bottom in each image, are from peaches with 24 h freezing, peaches with 1 h freezing, and reference sample peaches stored at room temperature.

types of cone cells, resulting in trichromatic vision. As each cone has a broad spectral sensitivity, hence responding to the (weighted) cumulative power across a range of wavelengths, different spectral power distributions can produce the same cone response and hence color sensation.[32] The phenomenon of metamerism has important consequences in, for example, the print and textile industries where so-called metameric color matches will appear the same under a particular type of illumination (e.g., daylight) but may appear different under alternative illumination sources (e.g., indoor fluorescent lighting).[33]

The phenomenon of metamerism can also be used to test the spectral output of an illuminator. Color cards containing swatches which are metameric color matches under daylight (or D65 spectrum) are used when testing the quality of photographic lighting.

As the MSI images across a wide range of wavelengths, it can detect metameric color matches quite easily. Pantone D65 metamerism test cards were imaged by the MSI. Figure 3a shows the test cards imaged using a standard RGB camera, in sunlight conditions, where the metameric color matches are largely indistinguishable to the eye. In Figure 3b, the MSI image at 633 nm is shown, where the color matches are again largely indistinguishable. In Figure 3c, the MSI image at 740 nm is shown, clearly distinguishing the metameric colors. Figure 3d shows the results of a clustering analysis performed on the basis of the 740 nm image.

Tomato Ripening Study. The ripeness of tomato fruit is generally assessed by a consumer visually based on color. From a commercial perspective, the grading, packing, and processing of tomato fruit requires automated systems with the ability to assess ripeness, and colorimetric methods are used to achieve this.[34,35]

Figure 4 shows an example of MSI imaging data that has been processed and used to determine whether sample tomatoes are unripe or ripe. Imaging was performed over the course of 7 days, and the resulting data cubes were compiled and analyzed using Spectronon software. Figure 5 shows a selection of results from this study. Clustering analysis allows for the distinction to be drawn between ripe and unripe tomatoes and the subsequent transition to ripeness as the study progressed. It may be seen from the cluster mapping of the images that there are 2 clusters specific to the tomatoes represented by a light shade and a dark shade that change as time passes. The dark shade that is more widespread on the tomatoes from day 1 may be interpreted as the cluster representing unripe tomatoes or partially unripe tomatoes. As the study progressed, those regions of the tomatoes that ripened transition to the lighter shaded cluster which represents ripeness. The third component calculated from PCA analysis shows a similar trend and is also interpreted as the component representing ripening. The SIMCA classification of tomatoes using MSI presented in Figure 4 is based on the initial PCA of the tomato images which allows for sorting of each pixel by its spectrum and the assignment of classes or category variables to the spectral data at each pixel or spatial position.

Peach Chill Injury. Chill injury occurs in fruits when they are stored below optimal temperatures, causing damage to the fruit and reducing quality and shelf life.[36] Multispectral imaging can be used to detect chill injury in fruits before it becomes visible to the naked eye.[37]

A study was conducted using the LED MSI to examine chill injury and its detection using a combination of multispectral imaging and multivariate analysis. Peaches were stored in a freezer for 1 and 24 h and were subsequently imaged along with peaches stored at room temperature. The resulting data cubes were prepared and analyzed using Spectronon software and the clustering and principal component analysis (PCA) modules it provides. In Figure 6, the results from the cluster analysis and the first two components calculated using PCA are presented along with imaging of the samples using illumination from a 586 nm

LED. The clustering results were calculated using 5 clusters to describe the image, and we can see that the damage caused by freezing of the fruit has been identified. PCA results show the manner in which individual components can be associated with features in the image; for instance, the chill injury exhibited by the peach samples is detected by the first component while the paper towel that was underneath the peaches is clearly identified by the second component. Examining the results from the multivariate analysis allows for identification of the wavelength of illumination in which the most useful information is found. In this instance, the illumination from the 586 nm LED produces an image that correlates with the findings from the multivariate analysis. In this way, devices that employ machine vision can be simplified. The ability to identify physical characteristics based on the combination of multispectral imaging and multivariate analysis techniques such as clustering and principal component analysis can be combined with classification methods such as "soft independent modeling of class analogies" or SIMCA for identification and sorting in machine vision based process analysis technology.

CONCLUSION

The MSI described here is a low-cost device, which is sufficiently simple in its construction and use, to become a useful tool in the teaching of undergraduate chemistry courses concerned with the concepts of spectroscopy,[16−18] chemometrics,[19−22] and colorimetry.[23,24] In addition, its analytical power is sufficient to tackle complex sample analysis tasks, which has been demonstrated through the analysis of chill injury in peach fruit. This makes the device suitable for independent student inquiry activities such as undergraduate projects. The construction of the device, including the interfacing of electronic hardware and control software, offers an opportunity for the hands-on development of student knowledge and skills in the areas of engineering, instrumentation, and automation.

ASSOCIATED CONTENT

Supporting Information

The Supporting Information is available at https://pubs.acs.org/doi/10.1021/acs.jchemed.0c00407.

Details of LED PCB components, control PCB components, cables and power supply, optical component dimensional drawings, alternative electronic control scheme overview, and overview of information included in ZIP file (PDF, DOCX)

LED and control PCB design files, mechanical part STL files, NI LabVIEW control program, programs for alternative electronic control scheme, and video of MSI in use (ZIP)

AUTHOR INFORMATION

Corresponding Author

Annemarie McCarthy − *Cork Institute of Technology, Bishopstown, Cork, Ireland*; orcid.org/0000-0002-3355-9965; Email: annemarie.mccarthy@cit.ie

Authors

Killian Barton − *Cork Institute of Technology, Bishopstown, Cork, Ireland*

Liam Lewis − *Cork Institute of Technology, Bishopstown, Cork, Ireland*; orcid.org/0000-0002-6600-4114

Complete contact information is available at: https://pubs.acs.org/10.1021/acs.jchemed.0c00407

Notes

The authors declare no competing financial interest.

ACKNOWLEDGMENTS

This work was funded in part by Science Foundation Ireland through the TIDA program (Grant 16/TIDA/4200).

REFERENCES

(1) Rajkó, R. *Techniques and Applications of Hyperspectral Image Analysis*; Grahn, H., Geladi, P., Eds.; Wiley: Chichester, 2007. *Journal of Chemometrics* **2008**, *22* (7), 441−442. DOI: 10.1002/cem.1159

(2) Cubero, S.; Aleixos, N.; Moltó, E.; Gómez-Sanchis, J.; Blasco, J. Advances in Machine Vision Applications for Automatic Inspection and Quality Evaluation of Fruits and Vegetables. *Food and Bioprocess Technology*; Springer, 2011; pp 487−504. DOI: 10.1007/s11947-010-0411-8

(3) Li, J. B.; Huang, W. Q.; Zhao, C. J. Machine Vision Technology for Detecting the External Defects of Fruits—A Review. *Imaging Science Journal* **2015**, *63*, 241−251.

(4) Slater, P. N. Survey of Multispectral Imaging Systems for Earth Observations. *Remote Sensing of Environment* **1985**, *17* (1), 85−102.

(5) Hagen, N.; Kudenov, M. W. Review of Snapshot Spectral Imaging Technologies. *Opt. Eng.* **2013**, *52* (9), 090901.

(6) Motorized Filter Wheels, Stepper Motor Driven. https://www.thorlabs.com/newgrouppage9.cfm?objectgroup_id=988 (accessed Apr 24, 2020).

(7) ZEISS Microscopy Online Campus|Interactive Tutorials|Filter Wheels. http://zeiss-campus.magnet.fsu.edu/tutorials/filterwheel/indexflash.html (accessed Apr 24, 2020).

(8) Acousto-Optic Tunable Filters—Java Tutorial|Olympus Life Science. https://www.olympus-lifescience.com/en/microscope-resource/primer/java/filters/aotf/ (accessed Apr 24, 2020).

(9) HySpex. https://www.hyspex.com/hyperspectral-imaging/what-is-hsi/ (accessed Apr 24, 2020).

(10) Bandpass Filter Kits. https://www.thorlabs.com/newgrouppage9.cfm?objectgroup_id=873 (accessed Apr 24, 2020).

(11) Commercial Snapshot Spectral Imaging: The Art of the Possible| The MITRE Corporation. https://www.mitre.org/publications/technical-papers/commercial-snapshot-spectral-imaging-the-art-of-the-possible (accessed Jun 29, 2020).

(12) Bolton, F. J.; Bernat, A. S.; Bar-Am, K.; Levitz, D.; Jacques, S. Portable, Low-Cost Multispectral Imaging System: Design, Development, Validation, and Utilization. *J. Biomed. Opt.* **2018**, *23* (12), 1.

(13) Christens-Barry, W. A.; Boydston, K.; France, F. G.; Knox, K. T.; Easton, Jr., R. L.; Toth, M. B. Camera System for Multispectral Imaging of Documents. In *Sensors, Cameras, and Systems for Industrial/Scientific Applications X*; Bodegom, E., Nguyen, V., Eds.; SPIE, 2009; Vol. *7249*, p 724908. DOI: 10.1117/12.815374

(14) Goel, M.; Whitmire, E.; Mariakakis, A.; Scott Saponas, T.; Joshi, N.; Morris, D.; Guenter, B.; Gavriliu, M.; Borriello, G.; Patel, S. N. HyperCam: Hyperspectral Imaging for Ubiquitous Computing Applications. In *UbiComp 2015—Proceedings of the 2015 ACM International Joint Conference on Pervasive and Ubiquitous Computing*; 2015; pp 145−156. DOI: 10.1145/2750858.2804282

(15) Everdell, N. L.; Styles, I. B.; Claridge, E.; Hebden, J. C.; Calcagni, A. S. Multispectral Imaging of the Ocular Fundus Using LED Illumination. In *Optics InfoBase Conference Papers*; Depeursinge, C. D., Vitkin, I. A., Eds.; Optical Society of America, 2009; Vol. *7371*, p 73711C. DOI: 10.1117/12.831769

(16) Sattar, S. Characterizing Color with Reflectance. *J. Chem. Educ.* **2019**, *96* (6), 1124−1128.

(17) Hoffman, E. M.; Beussman, D. J. Paint Analysis Using Visible Reflectance Spectroscopy. An Undergraduate Forensic Lab. *J. Chem. Educ.* **2007**, *84* (11), 1806−1808.

(18) Garrido-González, J. J.; Trillo-Alcalá, M.; Sánchez-Arroyo, A. J. Lights, Camera, Spectroscope! The Basics of Spectroscopy Disclosed Using a Computer Screen. *J. Chem. Educ.* **2018**, *95* (5), 903–907.
(19) Wang, L.; Mizaikoff, B.; Kranz, C. Quantification of Sugar Mixtures with Near-Infrared Raman Spectroscopy and Multivariate Data Analysis: A Quantitative Analysis Laboratory Experiment. *J. Chem. Educ.* **2009**, *86* (11), 1322–1325.
(20) de Oliveira, R. R.; das Neves, L. S.; de Lima, K. M. G. Experimental Design, near-Infrared Spectroscopy, and Multivariate Calibration: An Advanced Project in a Chemometrics Course. *J. Chem. Educ.* **2012**, *89* (12), 1566–1571.
(21) de Lorenzi Pezzolo, A. To See the World in a Grain of Sand: Recognizing the Origin of Sand Specimens by Diffuse Reflectance Infrared Fourier Transform Spectroscopy and Multivariate Exploratory Data Analysis. *J. Chem. Educ.* **2011**, *88* (9), 1304–1308.
(22) Rodríguez-Rodríguez, C.; Amigo, J. M.; Coello, J.; Maspoch, S. An Introduction to Multivariate Curve Resolution-Alternating Least Squares: Spectrophotometric Study of the Acid-Base Equilibria of 8-Hydroxyquinoline-5-Sulfonic Acid. *J. Chem. Educ.* **2007**, *84* (7), 1190–1192.
(23) Gee, C. T.; Kehoe, E.; Pomerantz, W. C. K.; Penn, R. L. Quantifying Protein Concentrations Using Smartphone Colorimetry: A New Method for an Established Test. *J. Chem. Educ.* **2017**, *94* (7), 941–945.
(24) Lisensky, G.; McFarland-Porter, R.; Paquin, W.; Liu, K. Synthesis and Analysis of Zinc Copper Indium Sulfide Quantum Dot Nanoparticles. *J. Chem. Educ.* **2020**, *97* (3), 806–812.
(25) Mabbott, G. A. Teaching Electronics and Laboratory Automation Using Microcontroller Boards. *J. Chem. Educ.* **2014**, *91* (9), 1458–1463.
(26) Albert, D. R. Constructing, Troubleshooting, and Using Absorption Colorimeters to Integrate Chemistry and Engineering. *J. Chem. Educ.* **2020**, *97* (4), 1048–1052.
(27) ERDC Knowledge Core: HyperCube Windows Executable. https://erdc-library.erdc.dren.mil/jspui/handle/11681/2920 (accessed Jun 25, 2020).
(28) Hyperspectral Imaging Application|Resonon. https://resonon.com/software (accessed Jun 29, 2020).
(29) Sengupta, A. A First Course in Machine Learning by Simon Rogers and Mark Girolami. *International Statistical Review* **2014**, *82* (1), 158–159.
(30) A One-Stop Shop for Principal Component Analysis—Towards Data Science. https://towardsdatascience.com/a-one-stop-shop-for-principal-component-analysis-5582fb7e0a9c (accessed Apr 24, 2020).
(31) K-means Clustering: Algorithm, Applications, Evaluation Methods, and Drawbacks. https://towardsdatascience.com/k-means-clustering-algorithm-applications-evaluation-methods-and-drawbacks-aa03e644b48a (accessed Apr 24, 2020).
(32) Karlicek, R.; Sun, C.-C.; Zissis, G.; Ma, R. *Handbook of Advanced Lighting Technology*; Springer, 2017.
(33) The Print Guide: The Issue of Metamerism in Print Production. http://the-print-guide.blogspot.com/2010/05/issue-of-metamerism-in-print-production.html (accessed Apr 24, 2020).
(34) López Camelo, A. F.; Gómez, P. A. Comparison of Color Indexes for Tomato Ripening. *Horticultura Brasileira* **2004**, *22* (3), 534–537.
(35) Polder, G.; van der Heijden, G. W. A. M.; Young, I. T. Hyperspectral Image Analysis for Measuring Ripeness of Tomatoes. In *2000 ASAE International Meeting*; 2000.
(36) Albornoz, K.; Cantwell, M. I.; Zhang, L.; Beckles, D. M. Integrative Analysis of Postharvest Chilling Injury in Cherry Tomato Fruit Reveals Contrapuntal Spatio-Temporal Responses to Ripening and Cold Stress. *Sci. Rep.* **2019**, *9* (1), 1–14.
(37) Pan, L.; Zhang, Q.; Zhang, W.; Sun, Y.; Hu, P.; Tu, K. Detection of Cold Injury in Peaches by Hyperspectral Reflectance Imaging and Artificial Neural Network. *Food Chem.* **2016**, *192*, 134–141.

https://dx.doi.org/10.1021/acs.jchemed.0c00407
J. Chem. Educ. 2020, 97, 3892–3898